Large-Scale Baroclinic Instability of the Mean Oceanic Circulation: A Local Approach

ANTOINE HOCHET, THIERRY HUCK, AND ALAIN COLIN DE VERDIÈRE

Laboratoire de Physique des Océans, Brest, France

(Manuscript received 7 May 2015, in final form 1 July 2015)

ABSTRACT

Large-scale baroclinic instability is investigated as a potential source of Rossby waves and large-scale variability in the ocean. This baroclinic instability is first reviewed in a 2.5-layer model. As already noticed by several authors, the instability arises in westward surface mean flow when the phase velocities of the two vertical modes are made equal by mean flow influence. This large-scale instability is stronger at low latitudes and thus is likely to happen in the westward return flow of the subtropical gyres. Further investigations with a continuous stratification quasigeostrophic model show that the instability is stronger where the mean flow projects negatively on the second baroclinic mode (imposing positive vertical modes at the surface). The linear stability calculation is then performed on Argo-derived mean flow along with mean stratification data. The results show that the unstable regions are situated at low latitudes in every oceanic basin, in western boundary currents, and in some part of the Antarctic Circumpolar Current. The location of these unstable regions is well correlated with the region of negative projection of the mean flow on the second baroclinic mode. Given that the unstable mode growth times are generally smaller than 6 months at low latitudes, these unstable modes are likely to be observable in satellite altimetry. Therefore, results of the present article suggest that the large-scale instability is indeed a source of large-scale variability at low latitudes.

1. Introduction

During the last 20 yr, the measurements of the ocean surface properties by satellite instruments have allowed us to significantly increase our knowledge of ocean dynamics. Chelton and Schlax (1996) were among the first to show that large-scale anomalies, propagating to the west, were observable in the altimetry. Since then, a large number of authors have described these anomalies, generally depicted as Rossby waves, using various techniques such as a Hovmöller diagram (Chelton and Schlax 1996), Fourier transform (Osychny and Cornillon 2004), finite impulse response (FIR) filter (Polito and Liu 2003), and so on. It is generally agreed that the large-scale anomalies can be seen in every oceanic basin (Fu 2004) and that their displacement velocity is in good agreement with Rossby wave phase velocity theory at latitudes lower than 30° (Polito and Liu 2003) but faster at higher latitudes (Chelton and Schlax 1996; Osychny and Cornillon 2004), especially for small wavelengths (Zang and Wunsch 2001). The discrepancy between the theory and satellite observations seems to be reduced by the inclusion of both the mean flow and the topography in the theory of Rossby waves (Killworth et al. 1997; Killworth and Blundell 2005; Aoki et al. 2009; Tailleux and McWilliams 2001; Hunt et al. 2012).

The Rossby waves can be forced by numerous phenomena such as the wind or buoyancy anomalies, mesoscale eddies, eastern boundary anomalies, and so on. In fact, they are the main response of the ocean to large-scale forcing, and as such, any process that introduces a large-scale perturbation in the ocean is likely to produce Rossby waves. White and Saur (1983) and more recently Fu and Qiu (2002) studied the respective role of wind variability and eastern boundary variability in setting the observed surface anomalies in the North Pacific. They found that the eastern boundary is mostly responsible for the variability at low latitudes, whereas wind forcing accounts for most of the signal at mid- and high latitudes. Cabanes et al. (2006) showed that in some regions of the North Atlantic, a large part of the large-scale signal is also related to the local response to heat flux changes.

In this article, we are particularly interested in the generation of Rossby waves, or more broadly of large-scale

Corresponding author address: Antoine Hochet, Laboratoire de Physique des Océans UMR 6523, UBO/UFR Sciences et Techniques 6 Avenue le Gorgeu, 29200 Brest, France.
E-mail: antoine.hochet@univ-brest.fr

DOI: 10.1175/JPO-D-15-0084.1

anomalies, by the baroclinic instability of the mean flow. Baroclinic instability is believed to be the main forcing of mesoscale eddies (Gill et al. 1974). Smith (2007) has performed a global stability analysis on the observed mean flow and has shown that most of the ocean is unstable, particularly regions of strong mean currents such as western boundary currents or the Antarctic Circumpolar Current. The fastest growing modes of this instability, called the Charney modes (Charney 1947), have growth rates of a few days and length scales generally smaller than 100 km. Smith (2007) also mention a good correlation of the maximum growth rate with the observed distribution of eddy kinetic energy.

However, as first shown by Green (1960), the mean flow can also be unstable at larger length scale; these unstable modes are called "Green modes." The method used in Smith (2007) filters out the Green modes by selecting the fastest growing modes. But this choice is not a suitable method for the study of these large-scale modes and a different method needs to be developed. Killworth and Blundell (2007) filters out the Charney modes by calculating the instability at specified zonal and meridional wavenumbers: $k = 2\pi/500\,\mathrm{rad\,km^{-1}}$ and $l = 0$. However, by imposing arbitrary wavelengths, this method is unlikely to select the fastest growing Green modes. Smith (2007) showed, for the Charney modes, that the wavenumbers at which the fastest growth occurred are quite sensitive to the mean flow direction and intensity. The same behavior is expected for the Green modes. Colin de Verdière (1986) and de Szoeke (1999) have discussed the conditions of baroclinic instability in the planetary geostrophic large-scale context. Colin de Verdière and Huck (1999) and Liu (1999) have shown that the mechanism behind the Green modes can conveniently be understood in a 2.5-layer quasigeostrophic (QG) model. At large scales, under the rigid-lid approximation, the time scale of the barotropic mode becomes infinitely small, while that of the baroclinic mode is very large, making these two modes unable to interact and give rise to an instability. This property of the barotropic motion explains why the large-scale instability does not happen in a 2-layer setting, while it is possible in a 2.5-layer model where two active baroclinic modes can interact.

A subsidiary question concerns the link of these unstable Green modes with the global unstable or least damped modes calculated in the ocean general circulation model by Sévellec and Fedorov (2013) for instance. These modes have decadal time scales and are good candidates to explain the decadal natural variability in ocean and coupled models. Sévellec and Huck (2015) interpreted this mode in a simplified three-level model as resulting from unstable large-scale baroclinic Rossby waves. However, our main theoretical tool to understand this phenomenon is precisely the local baroclinic instability analysis that gives rise to the Green modes. The questions we want to address therein are as follows: First, what is the mechanism of large-scale baroclinic instability? Which properties of the mean flow lead to such instability? And, finally, what are the regions, if any, where the mean flow circulation is most likely to produce large-scale instabilities?

We will first review the mechanism of large-scale baroclinic instability as depicted in Colin de Verdière and Huck (1999) and Liu (1999) and add some results useful for its understanding. Then, we will perform the stability calculation on real mean flow data extracted from a database constructed with Argo floats displacements (Ollitrault and Colin de Verdière 2014) and the thermal wind with the *World Ocean Atlas 2009* (*WOA2009*). The last sections conclude and give some perspectives for future work.

2. The 2.5-layer quasigeostrophic model

The best way to understand the mechanism of large-scale unstable modes is to use the simplest model where they can be found. The simplest model with large-scale baroclinic instability is the 2.5-layer QG model already studied by Liu (1999). The mean flow is assumed to be purely zonal in two active layers with the same thickness $H = 200$ m. Under the QG assumptions, the conservation of potential vorticity in layers 1 and 2 reads

$$\begin{cases} \dfrac{d}{dt}[\nabla^2\psi_1 + F_1(\psi_2 - \psi_1) + \beta y] = 0 \\ \dfrac{d}{dt}[\nabla^2\psi_2 + F_2(\psi_1 - 2\psi_2 + \psi_3) + \beta y] = 0 \end{cases}, \qquad (1)$$

with $F_1 = F_2 = F = f_0^2/(g'H)$ the squared inverse of the deformation radius, where g' is the reduced gravity and f_0 and β are, respectively, the Coriolis parameter and its local linear variation; $d\cdot/dt = \partial_t\cdot + J(\psi_i, \cdot)$ with $i = 1, 2$; and $\psi_n(x, y, t)$ $(n = 1, 2, 3)$ are the streamfunctions in layers 1, 2, and 3, respectively, with (x, y, t) the zonal, meridional, and time coordinates. We assume that there is no pressure anomaly in layer 3, which implies that $\psi_3 = 0$ in (1). Since we are interested in large-scale anomalies, the long-wave approximation is made. Furthermore, we also assume in what follows that the equations are inviscid and adiabatic. The use of the long-wave approximation implies that the equations have no dependence on wavenumber $||\mathbf{k}||$ and, as a result, the calculation of the phase speed and the effect of the dissipation (which is dependent on $||\mathbf{k}||$) can be treated

independently. We will only deal with the first problem in this article. System (1) thus becomes

$$\begin{cases}\left(U_1\dfrac{\partial}{\partial x}+\dfrac{\partial}{\partial t}\right)[F(\psi_2-\psi_1)]+[\beta+F(U_1-U_2)]\dfrac{\partial\psi_1}{\partial x}=0\\ \left(U_2\dfrac{\partial}{\partial x}+\dfrac{\partial}{\partial t}\right)[F(\psi_1-2\psi_2)]+[\beta+F(2U_2-U_1)]\dfrac{\partial\psi_2}{\partial x}=0\end{cases}, \tag{2}$$

which is the same as system (6) in Liu (1999). The quantities U_1 and U_2 are the mean velocities in layer 1 and 2, respectively. Introducing $\psi_i=\alpha_i\exp[j(kx-\omega t)]$ in (2), where i is the number of the layer, j is the imaginary unit, and assuming the meridional wavenumber $l=0$, lead to

$$\begin{cases}(U_1-c)[F(\alpha_2-\alpha_1)]+[\beta+F(U_1-U_2)]\alpha_1=0\\ (U_2-c)[F(\alpha_1-2\alpha_2)]+[\beta+F(2U_2-U_1)]\alpha_2=0\end{cases}. \tag{3}$$

System (3) has a solution only if its determinant is zero. The following second-order equation for $c=\omega/k$ is then obtained:

$$c^2F^2+cF(3\beta-FU_2)+\beta[\beta-F(U_1+U_2)]=0. \tag{4}$$

The solutions have an imaginary part only if the discriminant of (4) is negative. This discriminant, called Δ, is linked to the model parameters through the following formula:

$$\Delta=[5\beta^2+\beta F(4U_1-2U_2)+F^2U_2^2]F^2. \tag{5}$$

The phase velocities corresponding to the two solutions are then

$$c_\pm=\frac{-F(3\beta-FU_2)\pm\sqrt{\Delta}}{2F^2}. \tag{6}$$

Without mean flow, c_- is the first baroclinic mode while c_+ is the second. The vertical structures of the first and second baroclinic modes without mean flow satisfy

$$[G_1(1),G_1(2)]=[1,0.5(-1+\sqrt{5})] \tag{7}$$

for the first baroclinic mode with its phase velocity $c_1=-(\beta/F)[(3+\sqrt{5})/2]$ and

$$[G_2(1),G_2(2)]=[1,0.5(-1-\sqrt{5})] \tag{8}$$

for the second with $c_2=-(\beta/F)[(3-\sqrt{5})/2]$.

The equation $\Delta=0$ that separates the unstable solutions from the stable ones can be written as a parabola equation:

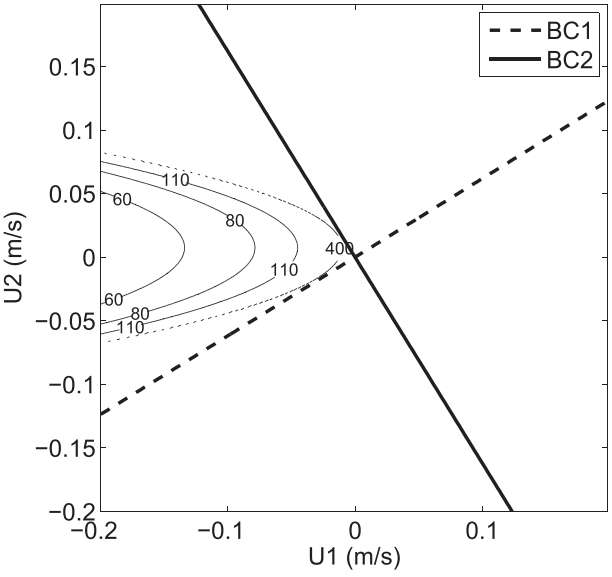

FIG. 1. Growth time (days) of large-scale modes in a 2.5-layer quasigeostrophic model as a function of the zonal velocities in layer 1 (U_1) and layer 2 (U_2). The zonal wavelength is 1000 km, and the latitude is 30°N. The two lines are the first (dashed) and second (solid) baroclinic modes; $H=200$ m.

$$U_1=-\frac{1}{4\beta F}[(FU_2-\beta)^2+4\beta^2]. \tag{9}$$

From this formula, it is a simple matter to show that the instabilities arise when both $U_1<-(\beta/F)$ and $|U_2-(\beta/F)|<\sqrt{-[(U_1F)/\beta]-1}$ are satisfied. Thus, the surface velocity needs to be directed westward to produce instabilities. When the surface zonal westward velocity is stronger, the growth time decreases and the instability becomes stronger. Figure 1 shows the growth time as a function of U_1 and U_2 calculated with a 1000-km zonal wavelength. The directions of the two vertical modes (with no mean flow) are shown on the same figure; the first baroclinic mode direction obeys the equation $U_1=0.5(1+\sqrt{5})U_2$ and that of the second mode obeys the equation $U_1=0.5(1-\sqrt{5})U_2$. The directions satisfy

$$\begin{pmatrix}U_1\\U_2\end{pmatrix}\begin{bmatrix}G_2(1)\\G_2(2)\end{bmatrix}=0 \tag{10}$$

for the first baroclinic mode and

$$\begin{pmatrix}U_1\\U_2\end{pmatrix}\begin{bmatrix}G_1(1)\\G_1(2)\end{bmatrix}=0 \tag{11}$$

for the second. We will explain in a following section why the unstable region is encompassed by these two directions.

a. Growth mechanism

What mechanism leads to an increase of the potential energy anomaly (the kinetic energy anomaly vanishes in the long-wave approximation)? By evaluating the magnitude of the different terms of the equation controlling the instability in a numerical experiment, Colin de Verdière and Huck (1999) have shown that the growth is dominated by $-\overline{b'v'}\partial_y B$, where b' is the anomaly of buoyancy, v' is the anomaly of meridional velocity, and B is the mean buoyancy. We show in what follows that this term can be obtained directly from the equation controlling the potential energy anomalies.

We write $\tau_1 = \psi_1 - \psi_2$ and $\tau_2 = \psi_2$, with τ_1 and τ_2 as the temperature anomalies respectively between layers 1 and 2 and between layers 2 and 3. Equations for τ_1 and τ_2 are

$$\begin{cases} \dfrac{F}{2}\dfrac{\partial\overline{\tau_1^2}}{\partial t} = -[\beta + F(U_1 - U_2)]\overline{\psi_2\dfrac{\partial\psi_1}{\partial x}} \\ \dfrac{F}{2}\dfrac{\partial\overline{\tau_2^2}}{\partial t} = \beta\overline{\psi_2\dfrac{\partial\psi_1}{\partial x}} \end{cases}, \tag{12}$$

where the mean over a wavelength is denoted by an upper bar.

For potential energies at each interface τ_1^2 and τ_2^2 to both have an exponential growth, then $\overline{\psi_2\partial\psi_1/\partial x} > 0$ and $[\beta + F(U_1 - U_2)] < 0$. One can check that the latter condition is indeed true in the instability region of Fig. 1 [$\beta + F(U_1 - U_2) = 0$ is the tangent to the parabola from (9) at $U_1 = -2\beta/F$ and $U_2 = -\beta/F$]. Since $\overline{\psi_2\partial\psi_1/\partial x} = -\overline{(\psi_1 - \psi_2)\partial\psi_1/\partial x} = \overline{b'\partial\psi_1/\partial x}$, the first condition implies positive eddy flux by the meridional velocity anomalies.

The equivalent relation for a continuous arbitrary stratification is

$$\frac{1}{2}\frac{\partial}{\partial t}\left[\overline{\left(\frac{\partial\psi}{\partial z}\right)^2}\right] = \overline{\frac{\partial U}{\partial z}\frac{\partial\psi}{\partial x}\frac{\partial\psi}{\partial z}}, \tag{13}$$

where the upper bar is now a mean over a wavelength and a mean over the depth. Therefore, a growth in the potential energy can only be achieved if $\overline{(\partial U/\partial z)(\partial\psi/\partial x)(\partial\psi/\partial z)} > 0$. One can check that the sum of (12) over the two active layers leads to the same relation. Note that (13) can be rewritten as

$$\frac{1}{2}\frac{\partial}{\partial t}\overline{b'^2} = -\overline{b'v'}\partial_y B. \tag{14}$$

This relation justifies the use of $\overline{b'v'}\partial_y B < 0$ in Colin de Verdière and Huck (1999) to diagnose baroclinic instability.

b. Latitude dependence

In the instability region, solutions [(6)] are complex conjugates and the growth time is calculated for a particular wavelength of $k = 2\pi/1000\,\text{km}$ as $1/\Im(\omega) = 1/[k\Im(c)]$ (where $\Im$ is the imaginary part). Here, we choose $H = 200\,\text{m}$ and $g' = 0.01\,\text{m s}^{-2}$. At 30°N, the growth time is approximately 150 days for a surface velocity of $1\,\text{cm s}^{-1}$ and 100 days when the velocity is $10\,\text{cm s}^{-1}$. The latitude dependence of the growth time is shown in Fig. 2 for a surface velocity of $U_1 = -2\,\text{cm s}^{-1}$ and for $U_2 = 0$. The growth time first decreases with the latitude until it reaches approximately 20° (for the mean velocities under consideration here), then the growth time increases rapidly and the waves become stable for smaller latitudes. This nonmonotonic behavior of the solution can be understood assuming $U_2 = 0$. Under this assumption, the mean flow is unstable wherever $U_1 < -(5/4)(\beta/F) = U_{1\text{min}}$. The latitude dependence of $U_{1\text{min}}$ is the same as that of the long Rossby waves' velocities, and when the latitude decreases, $U_{1\text{min}}$ becomes more negative and eventually reaches $-2\,\text{cm s}^{-1}$ at some latitude (here at 20°N); the flow is then stable. Figure 3 shows the latitude corresponding to the maximum growth as a function of U_1 and U_2. The larger the absolute values of U_1 and U_2, the lower the latitude of maximum growth. For reasonable mean flow values, we thus expect the large-scale instability to happen at low latitudes. These Figs. 1, 2, and 3 show that the unstable modes are found where the mean flow projects negatively on both baroclinic modes (when the vertical modes are chosen to be positive at the surface). The explanation of this feature will be given in a following section.

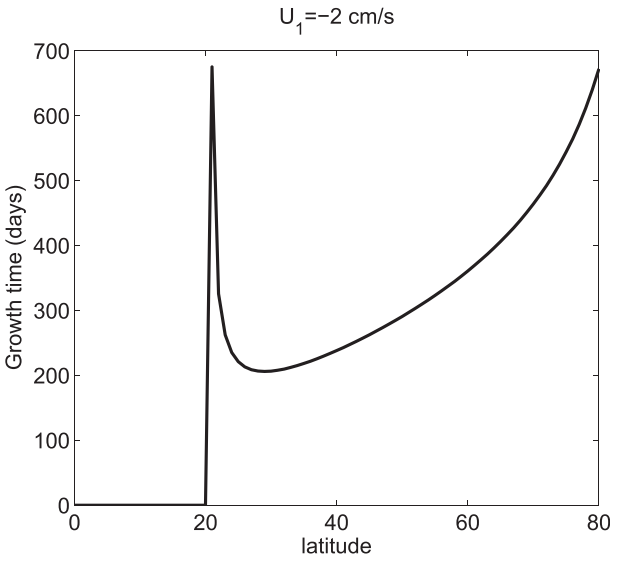

FIG. 2. Growth time (days) of large-scale modes in a 2.5-layer quasigeostrophic model as a function of the latitude for a zonal-surface velocity of $-0.02\,\text{m s}^{-1}$ and a zero velocity in layer 2. The zonal wavelength is 1000 km and $g' = 0.01\,\text{m s}^{-2}$; $H = 200\,\text{m}$.

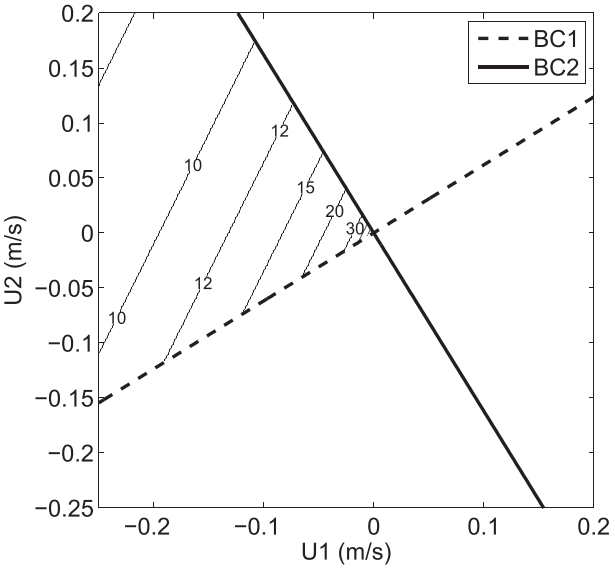

FIG. 3. Latitude of maximum growth for $H = 200$ m. The direction of the two vertical modes is added (dashed for the first baroclinic mode and solid for the second).

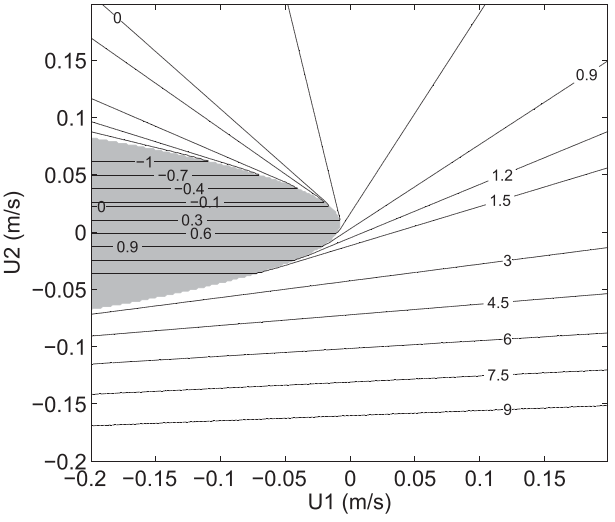

FIG. 4. Phase velocities of the fastest westward mode normalized by the phase velocity of the first baroclinic mode with no mean flow. The gray region shows the unstable region where $\Delta < 0$. The same figure (but for different parameters) can be found in Liu (1999).

c. *Phase speed variation*

The phase velocity of the fastest westward mode is shown in Fig. 4, which is adapted from Liu (1999) (normalized by the phase velocity of the first baroclinic mode with no mean flow) as a function of U_1 and U_2. For values of U_1 and U_2 situated in the instability region, there is one growing and one decaying mode with the same real phase velocity. The real phase velocity in the instability region depends solely on U_2:

$$C = -\frac{3\beta}{2F} + \frac{U_2}{2}. \tag{15}$$

When the mean flow is stable, Liu (1999) showed that one of the two modes approximately satisfies the "non-Doppler shift," whereas the second is advected by U_2. This effect can also be observed in Fig. 4. When U_2 is large enough toward the west, lines of the same phase velocities are aligned with those of U_2, whereas for $U_2 > 0$ and $U_1 > 0$, the phase velocity stays close to the baroclinic phase speed with no mean flow. The non-Doppler shift argument is then used in Liu (1999) to explain why the instability appears only where the first-layer velocity is westward. Liu first notes that an interaction between two baroclinic waves, and thus instability, is only possible when the two waves have the same phase speed. Assuming that U_1 and U_2 have the same sign, Liu (1999) argues that for a westward flow, one of the modes is advected toward the west, while the other is not modified (the first baroclinic mode), at least to leading order, because of the non-Doppler shift. As a result, the second baroclinic phase velocity can be equal to the first only if the flow is westward since an eastward flow would make the differences between the two phase speeds larger.

This argument, however, raises several questions such as what happens if $U_1 U_2 < 0$ since Fig. 1 shows that instabilities exist in this region? If the second baroclinic mode cannot reach the first baroclinic phase velocity with a westward flow, can the first baroclinic phase velocity be decelerated to reach the phase velocity of the second baroclinic mode? What happens when the number of vertical modes is increased? These questions will be answered in the next paragraphs.

d. *Can the first baroclinic Rossby wave phase speed be decreased by the mean flow toward the second baroclinic mode?*

First of all, let us show that the equality of the phase velocities of the two modes is a necessary condition for the instability but not a sufficient one. Indeed when the discriminant [(5)] is zero, the two modes (there is in fact only one mode) have the same phase velocity but are stable. Those modes are situated on the parabola [(9)].

Our goal in this paragraph is to derive an equation describing the evolution of the phase speeds of the two Rossby waves when the mean flow projects on the first or second baroclinic modes (calculated without mean flow). The vectors $G_1(z)$ and $G_2(z)$ form an orthogonal basis in which any anomaly can be expressed uniquely. As a result, ψ can be decomposed as

$$\begin{bmatrix} \psi_1(x,y,t) \\ \psi_2(x,y,t) \end{bmatrix} = a(x,y,t)G_1(z) + b(x,y,t)G_2(z),$$

where a and b are the coordinates of ψ in this basis.

Choosing to study the effect of a mean flow along $G_i(z)$ (where i can be 1 or 2), that is to say

$$\begin{pmatrix} U_1 \\ U_2 \end{pmatrix} = U_{\mathrm{BC}i} G_i(z),$$

and using the fact that the vertical modes without mean flow satisfy the following equation

$$-c_i \begin{Bmatrix} F[G_i(2) - G_i(1)] \\ F[G_i(1) - 2G_i(2)] \end{Bmatrix} + \beta \begin{bmatrix} G_i(1) \\ G_i(2) \end{bmatrix} = 0, \quad (16)$$

with $c_1 = -(3+\sqrt{5})[\beta/(2F)]$ and $c_2 = -(3-\sqrt{5})[\beta/(2F)]$, system (3) becomes

$$\begin{cases} [U_{\mathrm{BC}i} G_i(1) - c] F(\alpha_2 - \alpha_1) + \beta \left[1 - \dfrac{U_{\mathrm{BC}i}}{c_i} G_i(1)\right] \alpha_1 = 0 \\ [U_{\mathrm{BC}i} G_i(2) - c] F(\alpha_1 - 2\alpha_2) + \beta \left[1 - \dfrac{U_{\mathrm{BC}i}}{c_i} G_i(2)\right] \alpha_2 = 0 \end{cases}. \quad (17)$$

Using the decomposition of ψ on each vertical mode, system (17) becomes

$$\begin{cases} [U_{\mathrm{BC}i} G_i(1) - c]\beta \left[\dfrac{a}{c_1} G_1(1) + \dfrac{b}{c_2} G_2(1)\right] + \beta \left[1 - \dfrac{U_{\mathrm{BC}i}}{c_i} G_i(1)\right] [a G_1(1) + b G_2(1)] = 0 \\ [U_{\mathrm{BC}i} G_i(2) - c]\beta \left[\dfrac{a}{c_1} G_1(2) + \dfrac{b}{c_2} G_2(2)\right] + \beta \left[1 - \dfrac{U_{\mathrm{BC}i}}{c_i} G_i(2)\right] [a G_1(2) + b G_2(2)] = 0 \end{cases}. \quad (18)$$

Then, dividing by β and projecting on mode $G_i(z)$:

$$\left(-\frac{c}{c_i} + 1\right) a + b \sum_{j=1,2} G_i(j) G_1(j) G_2(j) U_{\mathrm{BC}i} \left(\frac{1}{c_2} - \frac{1}{c_1}\right) (-1)^{i+1} = 0, \quad (19)$$

and on the other mode $G_{3-i}(z)$,

$$0 + b\left(1 - \frac{c}{c_{3-i}}\right) + b \sum_{j=1,2} G_{3-i}(j) G_1(j) G_2(j) U_{\mathrm{BC}i} \left(\frac{1}{c_2} - \frac{1}{c_1}\right) (-1)^{i+1} = 0. \quad (20)$$

Equations (19) and (20) form a system of two equations with two unknowns that has a solution only if its determinant is zero. The zero determinant condition gives two solutions for c. The first is $c = c_i$, meaning that one of the two modes is not affected by the mean current; it is what has been called the non-Doppler shift. The remaining solution is

$$c = c_{3-i} + U_{\mathrm{BC}i} \left(1 - \frac{c_{3-i}}{c_i}\right) \sum_{j=1,2} G_{3-i}(j) G_1(j) G_2(j). \quad (21)$$

Since $G_1(2) > 0$, $G_2(1) > 0$, and $G_2(2) < 0$, the sum $\sum_{j=1,2} G_2(j) G_1(j) G_2(j)$ is positive; and since $G_1(1) G_1(1) G_2(1) > -[G_1(2) G_1(2) G_2(2)]$, the sum $\sum_{j=1,2} G_1(j) G_1(j) G_2(j)$ is also positive. The two waves have the same phase speed when $c = c_i$. Setting $c = c_i$ in (21) gives, with $i = 1$, the following mean zonal velocity on the first baroclinic mode:

$$U_{\mathrm{BC1}} = \frac{c_1}{\sum_{j=1,2} G_2(j) G_1(j) G_2(j)}. \quad (22)$$

And since $c_1 < 0$, U_{BC1} needs to be negative to make the two phase velocities equal. For a wave modified by a zonal mean flow with a second baroclinic vertical structure,

$$U_{\mathrm{BC2}} = \frac{c_2}{\sum_{j=1,2} G_1(j) G_1(j) G_2(j)}; \quad (23)$$

the same argument leads to the conclusion that $U_{\mathrm{BC2}} < 0$ when the two phase speed are equal. Thus, in order to decrease the westward phase velocity of the first baroclinic mode to make it equal to the second, the mean velocity needs to project negatively on the second baroclinic mode. However, if the mean current projects uniquely on a single vertical mode (which means that either $U_{\mathrm{BC1}} = 0$ or $U_{\mathrm{BC2}} = 0$), there is no instability. Indeed, (22) and (23) are situated on the parabola corresponding to a zero discriminant [(5)]. Figure 1 illustrates this property: when U_{BC} satisfies (23) and U_{BC1} satisfies (22), the two axes corresponding to the two vertical modes encompass the instability region. Therefore, in a 2.5-layer model, an instability can arise only if the projection of the mean flow is nonzero on the two vertical modes. We shall see, however, in section 3, that this property does not hold for configurations where the number of vertical modes is larger than two.

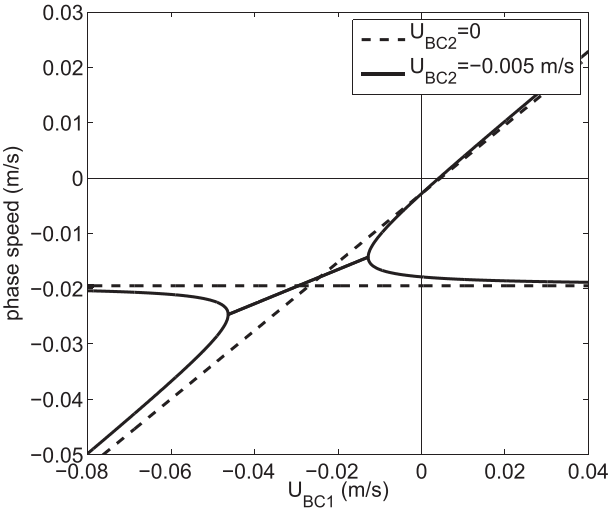

FIG. 5. Phase speed of the two modes as a function of the mean flow projection on the first baroclinic mode (U_{BC1}). The dashed line shows the phase speeds when the projection of the mean flow on the second baroclinic mode is zero, and the solid line shows when the projection is negative. The modes are unstable when there is only one solution for c (when $U_{BC2} < 0$).

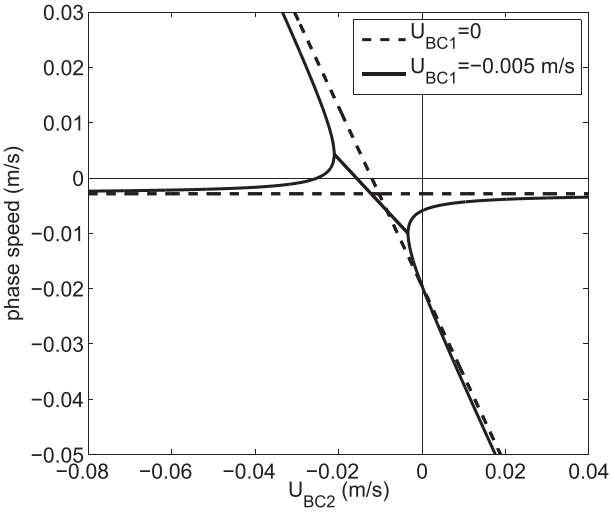

FIG. 6. As in Fig. 5, but for the second baroclinic mode (U_{BC2}).

As Liu (1999) suggested, the second baroclinic wave can be accelerated by a negative projection of the mean flow on the first baroclinic mode (which corresponds to a negative surface velocity). This possibility is illustrated in Fig. 5, where the mean flow contained in the first baroclinic mode accelerates the phase speed of the second baroclinic mode when it is negative and decelerates it otherwise. On the same figure, we show that when the mean flow projects negatively on the second baroclinic mode, an instability appears for $U_{BC1} < 0$, but that when the projection on the second baroclinic mode is zero, there is no instability. However, a second possibility that was not explored by Liu (1999) exists: the first baroclinic wave can be decelerated by a negative projection of the mean flow on the second baroclinic mode. This negative projection corresponds to a westward surface velocity and an eastward velocity in the second layer. This possibility is illustrated in Fig. 6 where the mean flow contained in the second baroclinic mode decelerates the phase speed of the first baroclinic mode when it is negative and accelerates it otherwise. In the same figure we show that when the mean flow projects negatively on the first baroclinic mode, an instability appears for $U_{BC2} < 0$, but when the projection on the first baroclinic mode is zero, there is no instability.

This second possibility has already been noticed by Dewar (1998) when trying to understand the discrepancy between the observed and theoretical planetary waves' phase speeds. The corrections of the phase velocities of the first baroclinic mode due to the mean flow are anticorrelated with the surface mean flow direction. This has been also observed in the continuous case by Colin de Verdière and Tailleux (2005).

e. *Vertical structure of the modes, link with their phase speed*

1) UNSTABLE REGION

Inside the unstable region shown in Fig. 1, the amplitude of the growing modes in the first layer $|\alpha_1|$ and in the second layer $|\alpha_2|$ can be linked using the phase speed [(6)] and the first equation of (3) for instance. The following formula is then obtained:

$$|\alpha_1| = -\frac{\beta + FU_1}{\beta}|\alpha_2|, \tag{24}$$

which shows that the ratio of the two amplitudes depends solely on the mean zonal velocity in the first layer. Thus, in the 2.5-layer model, the vertical structure of the modes inside the unstable region can project on the first or on second baroclinic mode depending on U_1.

2) STABLE REGION

We will first show that the curves of constant phase speed $c_i(U_1, U_2) = \text{constant}$ ($i = 1, 2$) are the straight lines tangent to the parabola $\Delta = 0$ [see (5), which links Δ to U_1 and U_2; there are two solutions]. The non-Doppler shift tells us that inside the stable region, c_i is unchanged if (U_1, U_2) is replaced by $(U_1, U_2) + \gamma(\alpha_1^i, \alpha_2^i)$, where γ is any real number and (α_1^i, α_2^i) is the eigenvector of system (3). Indeed, the advection of

the potential vorticity anomaly by the mean flow, $\gamma F[\alpha_1^i(\alpha_2^i - \alpha_1^i), \alpha_2^i(\alpha_1^i - 2\alpha_2^i)]$, cancels with the advection of mean potential vorticity by the meridional velocity anomaly $\gamma F[(\alpha_1^i - \alpha_2^i)\alpha_1^i, (2\alpha_2^i - \alpha_1^i)\alpha_2^i]$ in system (3).

As a result, the curves $c_i(U_1, U_2) = \text{constant}$ are straight lines directed by the vector (α_1^i, α_2^i). When the coefficient γ varies in $(U_1, U_2) + \gamma(\alpha_1^i, \alpha_2^i)$, one of the solutions c_i is unchanged, while the other c_{3-i} takes every value on the real number line, since c_{3-i} is of the form $A\gamma + B$, where A and B are constants depending on (U_1, U_2). The fact that c_{3-i} is of the form $A\gamma + B$ has been shown for the special case where $(U_1, U_2) = (0, 0)$ by (21), but the demonstration is essentially the same when $(U_1, U_2) \neq (0, 0)$. Thus, for some $\gamma_0 = \gamma_0$, we obtain $c_i = c_{3-i}(\gamma_0)$, which is situated on the parabola $\Delta = 0$. The equation $c_i(U_1, U_2) = \text{constant}$ is thus a straight line passing through the point (U_1, U_2) and a point situated on the parabola $\Delta = 0$. Furthermore, since $c_{3-i}(\gamma)$ can only be real (because c_i is real and c_i, c_{3-i} are the solutions to a second-order algebraic equation), the straight line of constant c_i does not cross the curve $\Delta = 0$ and is thus a tangent to this curve. As a result, in the plane (U_1, U_2) one can geometrically construct the constant phase speed lines and deduce from their slope the vertical structure of the modes. This is done in Fig. 7 where the constant phase speed lines are constructed as the tangents of the parabola $\Delta = 0$. Some modes are surface intensified (when the absolute slope is smaller than 1), while others are intensified in the second layer (when the absolute slope is larger than 1). This figure allows us to easily deduce several features of the influence of the mean zonal flow on the phase speed and vertical structure of the modes. Some of them will now be given.

When the phase velocity is larger than $-\beta/F$, the signs of the streamfunction in layers 1 and 2 are opposed, whereas they are otherwise of the same sign. When $U_1 = -\beta/F$, the phase velocity is westward, and the amplitude of one of the two modes is zero in the first layer. An example of this is shown in Fig. 7 by a black circle; for this particular mean velocity, one vertical mode is surface intensified while the other has a nonzero amplitude only in the second layer.

The two vertical modes both have the same sign in layers 1 and 2 when $U_1 < -\beta/F$, while they have opposite signs when $U_1 > -\beta/F$. The two tangents with thick black lines show the limits between the surface and second-layer intensified modes. Inside the region delimited by these two tangents (toward small $|U_1|$), one mode is intensified in the first layer and the other in the second layer. Outside this region (toward small $|U_2|$), the two modes are surface intensified.

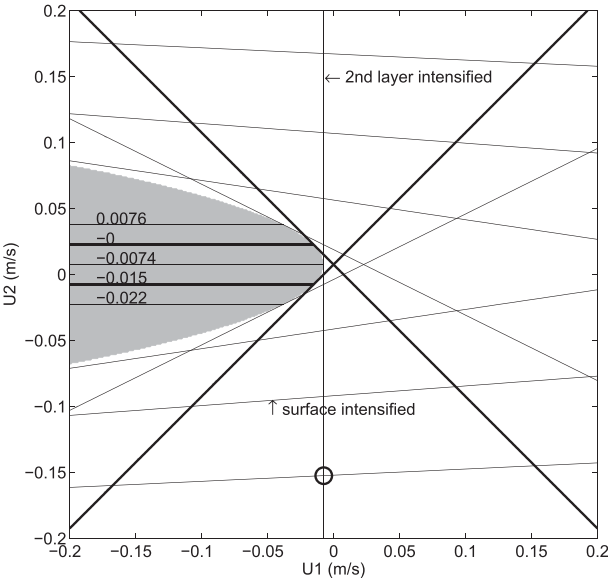

FIG. 7. Lines of constant phase speed (thin black lines) as a function of U_1, U_2. These straight lines are also the tangents to equation $\Delta = 0$. The gray region shows the region where $\Delta \leq 0$. As shown in section 2e, the slope of the straight lines reveals the vertical structure of the modes; when the absolute slope is larger than 1, the mode is second layer intensified, while when the slope is smaller than 1, the mode is surface intensified. The separations between surface- and second layer–intensified modes are given by the two thick black lines. Two examples are denoted by surface intensified or second layer intensified in the figure. The values of the phase velocities (in m s^{-1}) can conveniently be calculated by (15) on the parabola $\Delta = 0$, and some of them are reported in the figure in the $\Delta < 0$ region. The black circle shows a position (U_1, U_2) where one of the two modes is surface intensified, and the other is intensified in the second layer and is, in fact, completely contained in it.

3. Quasigeostrophic model with continuous vertical stratification

We have seen in the last section that the instability can arise in a 2.5-layer configuration either when the mean flow accelerates the second baroclinic mode or decelerates the first baroclinic mode. Both of these processes involve a westward zonal mean flow at the surface. However, one can ask if this is still the case when the number of vertical modes is increased. For instance, the inclusion of a third baroclinic mode makes the instabilities' possibilities potentially richer; the third baroclinic mode may also interact with the other two to give rise to an instability. We investigate this possibility in a continuously stratified model with a number of vertical modes determined by the number of vertical points (which is chosen to be 100 here). Assuming that the mean flow is zonal and that the long-wave approximation can be made, the linearized quasigeostrophic equation is

$$\left[\frac{\partial}{\partial t}+U(z)\frac{\partial}{\partial x}\right]\left\{\frac{\partial}{\partial z}\left[\frac{f_0^2}{N^2(z)}\frac{\partial\psi}{\partial z}\right]\right\}+\left\{\beta-\frac{\partial}{\partial z}\left[\frac{f_0^2}{N(z)^2}\frac{\partial U}{\partial z}\right]\right\}\frac{\partial\psi}{\partial x}=0, \quad (25)$$

with the following boundary conditions:

$$\left[\frac{\partial}{\partial t}+U(z)\frac{\partial}{\partial x}\right]\frac{\partial\psi}{\partial z}-\frac{\partial U}{\partial z}\frac{\partial\psi}{\partial x}=0, \quad (26)$$

which applies at $z = 0$ and $z = -H$. To study the effect of the vertical structure of $U(z)$ on the stability, $U(z)$ is written as a sum of the first and second baroclinic modes:

$$U(z)=U_{\mathrm{BC1}}F_1(z)+U_{\mathrm{BC2}}F_2(z), \quad (27)$$

where (U_{BC1}, U_{BC2}) are respectively the projection of $U(z)$ on the first and second baroclinic modes. The terms $F_1(z)$ and $F_2(z)$ are normalized at the surface [$F_1(0) = F_2(0) = 1$]. The mean flow is assumed to have a zero projection on higher baroclinic modes. The barotropic velocities, let us call them U_{BT} here, do not have any influence on the growth time since their only effect is to introduce a Doppler shift in the phase velocities: $C_{\mathrm{BT}} = C - U_{\mathrm{BT}}$, where C and C_{BT} are, respectively, the phase velocities (which can be imaginary) without and with the barotropic velocity.

Perturbation of the form $\psi(x, z, t) = \alpha(z)\exp[j(kx = \omega t)]$ is inserted in (25) and (26). It is straightforward to notice that (25) and (26) impose the frequency ω to be linear in k, that is, $\omega = -ck$ with c a constant. Thus, we simply calculate c and obtain the growth time: $T = 1/[\Im(\omega)]$ for a fixed k (here, and in what follows, we choose $k = 2\pi/1000\,\mathrm{rad\,km^{-1}}$).

The vertical profile of the buoyancy frequency is the one used in Gill et al. (1974):

$$N(z)=10^2 f_0\exp(z/1800), \quad (28)$$

where f_0 is the Coriolis parameter. The growth time of the most unstable mode as a function of U_{BC1} and U_{BC2} is shown in Fig. 8. Instabilities now arise everywhere in the (U_{BC1}, U_{BC2}) plan, but some of them, those for which $U_{\mathrm{BC2}} < 0$, have very short growth time. In contrast with the 2.5-layer configuration, strong instabilities with growth time shorter than a year can also happen for an eastward zonal surface (baroclinic) velocity. When the mean flow has a zero projection on the first baroclinic mode ($U_{\mathrm{BC1}} = 0$), the mean flow is unstable where $U_{\mathrm{BC2}} < 0$. Thus, unlike what have been found in the 2.5-layer configuration, in a continuous configuration, an instability can arise even if the mean flow projects on a single vertical mode.

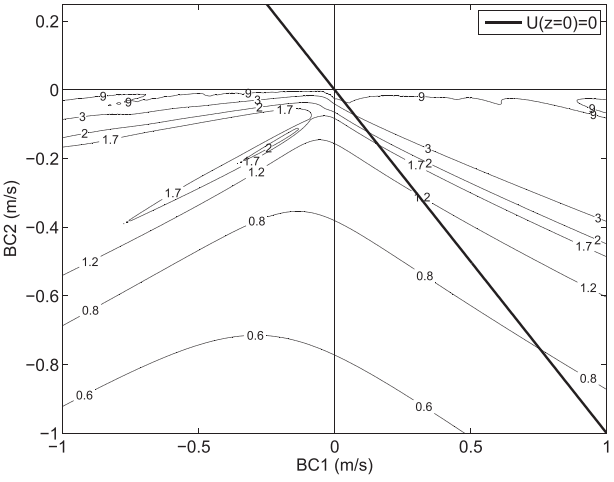

FIG. 8. Growth time (yr) of the most unstable mode in a continuously stratified QG model for a zonal mean flow $U(z) = U_{\mathrm{BC1}}F_1(z) + U_{\mathrm{BC2}}F_2(z)$ with $F_1(z)$, $F_2(z)$ the first and second baroclinic modes normalized at the surface [$F_1(0) = F_2(0) = 1$] and U_{BC1}, U_{BC2} the abscissa and ordinate multiplying these vertical structures. Instabilities happen everywhere, but only the growth time shorter than 9 yr are shown. The solid line represents $U(z = 0) = 0$; left of this line, $U(z = 0) < 0$, and right of this line, $U(z = 0) > 0$. The latitude under consideration is 30°N, and the buoyancy frequency is given by the analytical equation (28).

This can be explained by noticing that the 2.5-layer configuration is a singular one. Indeed, the instability is the result of the interaction of two waves, but when the mean flow projects on a single vertical mode, one of the two frequencies is real; unmodified by the mean flow (the non-Doppler shift mode), the remaining solution can thus only be real since both obey a second-order algebraic equation with real coefficients.

The fact that the instability is stronger for $U_{\mathrm{BC2}} < 0$ can conveniently be understood by assuming $U_{\mathrm{BC1}} = 0$ in a simpler three vertical modes model. A derivation of the N-layer model can be found in Flierl (1978). The use of a three vertical modes model instead of the continuous equations derived above [see (25)] simplifies the understanding of the instability mechanism by reducing the number of possible interactions. The variation of the phase velocities of the three baroclinic modes is shown in Fig. 9. The figure illustrates that with $U_{\mathrm{BC2}} > 0$, the phase velocities of the first and third baroclinic modes both increase westward but diverge. On the contrary, with $U_{\mathrm{BC2}} < 0$, the phase velocity of the third vertical mode increases, whereas that of the first vertical mode decreases. Thus, for some value of $U_{\mathrm{BC2}} < 0$, the two phase velocities are equal and an instability can develop. The projection of the vertical structures of the perturbations on the traditional vertical modes reveals that they are mostly contained in the first and second baroclinic modes.

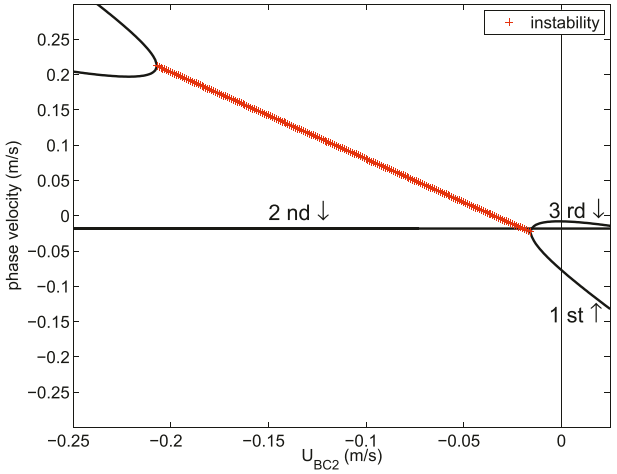

FIG. 9. The phase speed of first three baroclinic modes as a function of the projection of the mean flow on the second baroclinic vertical mode [normalized such that $(1/H)\int_{-H}^{0} G(z)^2\,dz = 1$ and $G(0) > 0$ with $G(z)$ the vertical mode under consideration]. The instabilities are shown with the thick red line made of red crosses. This calculation has been performed in a three modes model (first, second, and third baroclinic modes) described in Flierl (1978). The position of the three modes are shown in the figure; note that the phase speed of the second baroclinic mode is constant since the mean flow projects only on the second baroclinic mode.

The best way to find the regions in the ocean where these instabilities may arise is to perform the stability calculation directly on density and velocity profiles. This is the subject of the following section.

4. Stability of the oceanic mean flow currents as deduced from Argo floats

a. Method

First, (25) and (26) are modified to take into account both the zonal and meridional mean velocities $U(z)$ and $V(z)$:

$$\left[\frac{\partial}{\partial t} + U(z)\frac{\partial}{\partial x} + V(z)\frac{\partial}{\partial y}\right]\left\{\frac{\partial}{\partial z}\left[\frac{f_0^2}{N^2(z)}\frac{\partial \psi}{\partial z}\right]\right\} + \left\{\beta - \frac{d}{dz}\left[\frac{f_0^2}{N^2(z)}\frac{dU}{dz}\right]\right\}\frac{\partial \psi}{\partial x} - \frac{d}{dz}\left[\frac{f_0^2}{N^2(z)}\frac{dV}{dz}\right]\frac{\partial \psi}{\partial y} = 0, \tag{29}$$

with the following boundary condition

$$\left(\frac{\partial \bullet}{\partial t} + U\frac{\partial \bullet}{\partial x} + V\frac{\partial \bullet}{\partial y}\right)\frac{\partial \psi}{\partial z} - \frac{\partial \psi}{\partial y}\frac{dV}{dz} - \frac{\partial \psi}{\partial x}\frac{dU}{dz} = 0, \tag{30}$$

which applies at $z = 0$ and $z = -H$. Note that the boundary conditions in a realistic ocean are still debatable (see, for instance, Aoki et al. 2009; Bobrovich and Reznik 1999; Hunt et al. 2012; Tailleux and McWilliams 2001).

The mean flow database that is used to solve (29) has been constructed as follows: The mean geopotential at all depths is obtained by integrating hydrostatics from the absolute geopotential at 1000 db computed by Ollitrault and Colin de Verdière (2014) from Argo float displacements. The mean density field comes from the *WOA2009* (Locarnini et al. 2010; Antonov et al. 2010). The mean geostrophic currents have a 1° horizontal resolution and 33 vertical levels ranging from 10 m at the surface to 500 m at depth.

For each grid point on the globe, the mean current (U, V) and the stratification is extracted from the atlas, and

$$\frac{dQ}{dy} = \beta - \frac{d}{dz}\left[\frac{f_0^2}{N^2(z)}\frac{dU}{dz}\right]$$

and

$$\frac{dQ}{dx} = \frac{d}{dz}\left[\frac{f_0^2}{N^2(z)}\frac{dV}{dz}\right]$$

are calculated. Although $U \gg V$ in most of the ocean, the mean meridional velocity might play an important role in setting the largest growth rate at some places (see, for instance, Spall 2000). Once these fields are obtained, $\psi = \alpha(z)\exp[j(kx + ly + \omega t)]$ is introduced in (29), and the result is vertically discretized with centered finite differences. To solve (29), we write $\mathbf{k} = \|\mathbf{k}\|[\cos(\theta), \sin(\theta)]$, with θ as the orientation of the wave vector and $\|\mathbf{k}\|$ as its norm. Using $c = -\omega/\|\mathbf{k}\|$, (29) becomes

$$[-c + U\cos(\theta) + V\sin(\theta)]\left[\frac{\partial}{\partial z}\left(\frac{f_0^2}{N^2}\frac{d\alpha}{dz}\right)\right] + \left[\beta - \frac{d}{dz}\left(\frac{f_0^2}{N^2}\frac{dU}{dz}\right)\right]\cos(\theta)\alpha - \frac{d}{dz}\left(\frac{f_0^2}{N^2}\frac{dV}{dz}\right)\sin(\theta)\alpha = 0, \tag{31}$$

and the boundary condition at $z = 0$ and $z = -H$ is

$$[-c + U\cos(\theta) + V\sin(\theta)]\frac{d\alpha}{dz} - \sin(\theta)\alpha\frac{dV}{dz} - \cos(\theta)\alpha\frac{dU}{dz} = 0. \tag{32}$$

At each position, (31) and (32) are solved for θ varying between 0 and 2π. The $c(\theta)$ with the larger negative imaginary part is the fastest growing mode of the studied

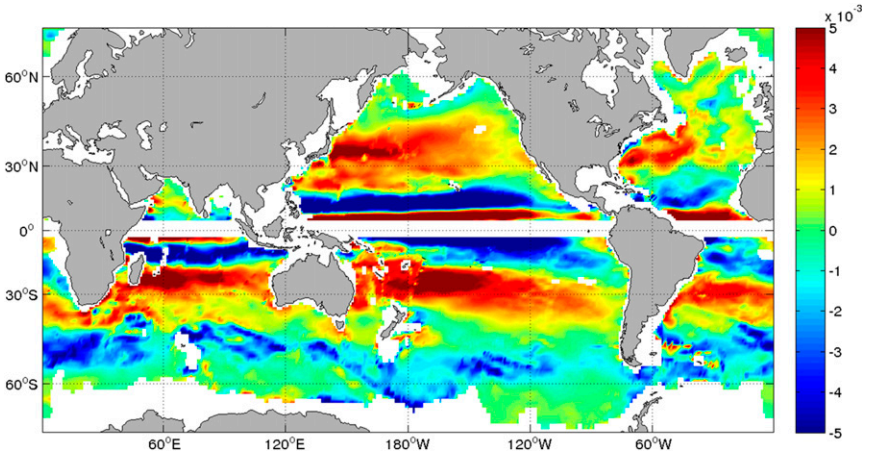

FIG. 10. Projection of the zonal mean flow ($\mathrm{m\,s^{-1}}$) on the second baroclinic mode [normalized by $(1/H)\int_{-H}^{0} G_2(z)^2\,dz$ with $G_2(z)$ as the second baroclinic vertical mode] calculated with stratification data from the *World Ocean Atlas 2009*.

position. The growth time $T = (c_{\max} k_m)^{-1}$ is obtained by multiplying $c_{\max}$ (the imaginary part of the fastest growing mode) and $k_m = 2\pi/1000\,\mathrm{rad\,km^{-1}}$.

To anticipate where the stronger instabilities take place, one can project the zonal mean flow on the second baroclinic mode [normalized such that $(1/H)\int_{-H}^{0} G(z)^2\,dz = 1$ and $G(0) > 0$, with $G(z)$ as the vertical mode under consideration] and look for regions where this projection is negative, as suggested in the previous section. This is done in Fig. 10, where the zonal mean flow is taken from the database that has been described above and has been projected on the second baroclinic mode. The vertical modes are calculated from *WOA2009* stratification data. The projection is negative at low latitudes and in some parts of the Antarctic Circumpolar Current.

b. Growth time and location of the unstable regions

The growth times given by this calculation {with $[U(z), V(z)]$} are shown in Fig. 11. The most unstable regions are situated at low latitudes in the Indian, Pacific, and Atlantic Oceans, with growth time scales shorter than a year. At higher latitudes, unstable regions exist mainly in the western boundary currents, particularly in the Gulf Stream and in the Antarctic Circumpolar Current. This figure confirms the conclusions of the 2.5-layer model studied above: large-scale instability is stronger at low latitudes.

A good correlation is found between the regions where the mean flow projects negatively on the second baroclinic mode (Fig. 10) and the regions of maximum growth (Fig. 11). Indeed the projection is negative in the ACC region and at low latitudes in the Indian, Atlantic, and Pacific Oceans, where the instability is strong. However, some regions are unstable; while the projection of the mean flow on the second baroclinic mode is positive, this is the case, for instance, of some part of western boundary currents. This is probably because the meridional mean flow, which is of the order of the zonal one in this region, was not taken into account in the previous stability criteria. At high latitudes, in the Atlantic and Pacific Oceans, the projection is negative in some regions that nevertheless remain stable. This is well explained by the fact that the higher the latitude, the smaller the instability, as shown in Fig. 2 in the 2.5-layer equations (an argument that is also valid with a vertically continuous stratification). Thus, for a given growth time, the negative projection of the mean flow on the second baroclinic mode is larger at high than at low latitudes. It explains why although these two regions are located at the same (absolute) latitude, the weak second baroclinic mode mean flow of the high-latitude regions of the North Pacific and Atlantic are stable, while the strong second baroclinic mode mean flow of the ACC is unstable.

c. Real phase speed of the unstable modes

The zonal average of the real phase speed of the most unstable wave as a function of the latitude for every oceanic basin is shown in Fig. 12 along with the phase speed of the fastest westward mode. Both phase speed are calculated with (31), but the former is chosen as the maximum of $\Im(c_i)$ (with i as the vertical mode number and $\Im$ as the imaginary part), while the latter is the minimum of $\Re(c_i)$ ($\Re$ is the real part).

This figure reveals that in every oceanic basin (Atlantic, Pacific, and Indian) and at mid- and high latitudes, the zonal phase speed of the most unstable mode follows quite well the phase speed of the fastest westward mode. At lower latitudes, the most unstable mode

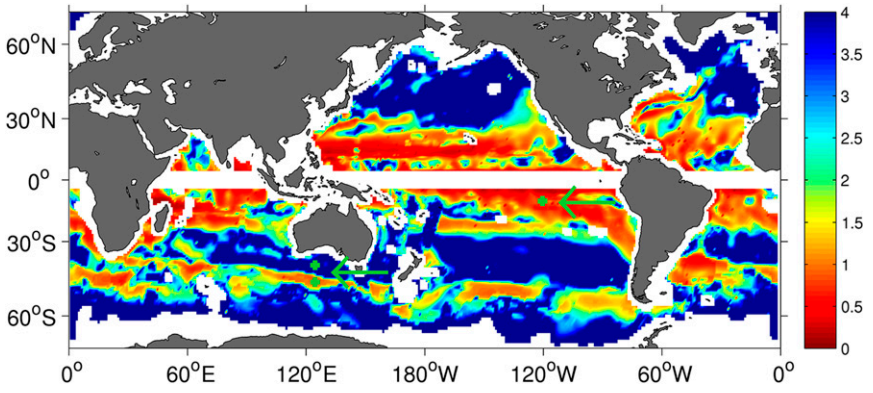

FIG. 11. Growth time $(\|\mathbf{k}\|c_i)^{-1}$ (yr) of the most unstable large-scale modes with $\|\mathbf{k}\| = 2\pi/1000\,\text{rad km}^{-1}$. The two green arrows show the three sites detailed in Figs. 15, 16, and 17 (precisely located with crosses). White regions are regions with no data.

phase speed is slightly smaller than that of the fastest westward mode but remains comparable. Since the observed phase speed are in good agreement with the fastest westward mode at low latitudes (Killworth et al. 1997), the phase speeds of the most unstable modes are also similar to that given by the observations.

A natural question then arises: is the growth rate sufficiently fast compared to the propagation time to produce an observable signal by, for instance, satellite altimetry? With a phase speed equal to $5\,\text{cm s}^{-1}$ (which is the phase speed around 20° of latitude), the time to cross a 4000-km basin is approximately 2.5 yr. Since the growth time in unstable regions may be shorter than 6 months, we expect the growth to be sufficiently large to be detectable in the altimetry. For instance, in this particular example, the amplitude of the initial perturbation is multiplied by $\exp(5) \approx 150$, and an initial perturbation amplitude as small as 1 mm could thus be seen in the satellite altimetry [which has a sampling error of 2–4 cm (Fu and Cazenave 2000)]. Of course, this argument assumes that the mean flow does not change along the mode propagation, which is generally not true. Nevertheless, at low latitudes the unstable regions seem to be sufficiently large (for instance the unstable region of the North Pacific extends from the U.S. West Coast to the Philippines) to allow a substantial growth.

d. *Vertical structure of the unstable modes*

For each spatial position, the vertical structure of the most unstable mode is projected on the local first and second baroclinic modes with no mean flow (and normalized such that that $(1/H)\int_{-H}^{0} G(z)^2\,dz = 1$ and $G(0) > 0$, with $G(z)$ as the vertical mode under consideration). The fraction of the vertical structure in the first and

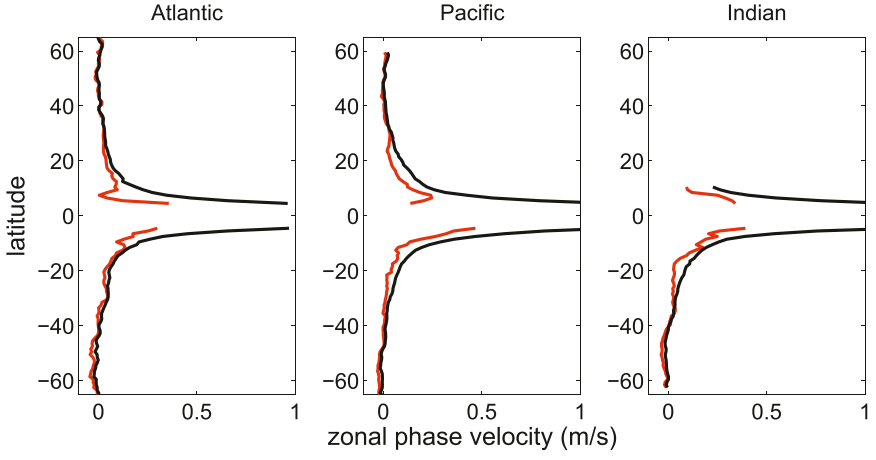

FIG. 12. Zonally averaged zonal phase speed (real part; m s^{-1}) of the most unstable mode (red) and of the fastest westward mode (black) for the (left) Atlantic, (center) Pacific, and (right) Indian Oceans as a function of the latitude. The phase velocities are calculated with Argo floats–derived mean flow data and with *WOA2009* stratification.

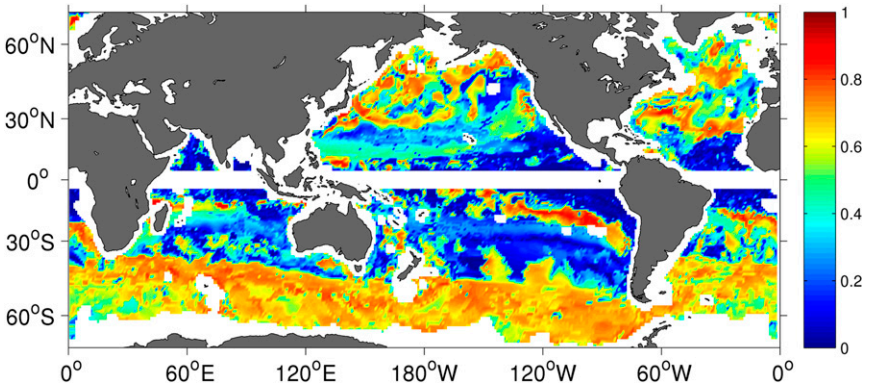

FIG. 13. Fraction of the most unstable mode vertical structure contained in the first baroclinic mode. The first baroclinic mode is calculated with *WOA2009* stratification, and the most unstable modes are calculated with Argo floats–derived mean flow. White regions are regions with no data.

second baroclinic modes is shown in Figs. 13 and 14. The vertical structure in the unstable regions is very well described by the first and second baroclinic modes. Indeed, the sum of these two modes represents more than 80% of the most unstable mode vertical structure in almost all regions. The ACC and part of the low-latitude South Pacific are mostly described by the first baroclinic mode. Low-latitude South Atlantic and part of the low-latitude South Pacific are mostly described by the second baroclinic mode. And finally, the Northwest Pacific is well described by both the first and second baroclinic modes. The vertical structure of the most unstable mode gives an idea of how the mode will be radiated if it reaches a stable region. For instance, a mode with a first baroclinic vertical structure leaving an unstable region will be radiated as a first baroclinic Rossby wave.

In Fig. 11, two arrows point toward three sites that are studied in detail in the following paragraph. These two regions are located in the Antarctic Circumpolar Current and at low latitude in the South Pacific Ocean. In each region, the mean meridional and zonal velocities are shown along with the amplitude and phase of the most unstable modes.

e. *Antarctic Circumpolar Current region*

The first site at 51°S and 124°E is situated in the ACC in one of the unstable regions of Fig. 11, south of Australia. The mean zonal velocity, shown in Fig. 15, is directed toward the east for all depths. It is at its maximum at the surface with a $10\,\mathrm{cm\,s^{-1}}$ value and decreases monotonically with depth. The meridional velocity is directed toward the south with a smaller amplitude of $2.5\,\mathrm{cm\,s^{-1}}$. The most unstable mode has a growth time of 0.4 yr and a vertical structure that follows a first baroclinic mode; it has one zero on the vertical around a depth of 1500 m. Although hardly noticeable in Fig. 15, the mean zonal velocity at this site has a negative projection on the second baroclinic mode. For comparison, we also show in Fig. 16 a site situated at the same longitude but at a lower latitude of 47°S, outside the

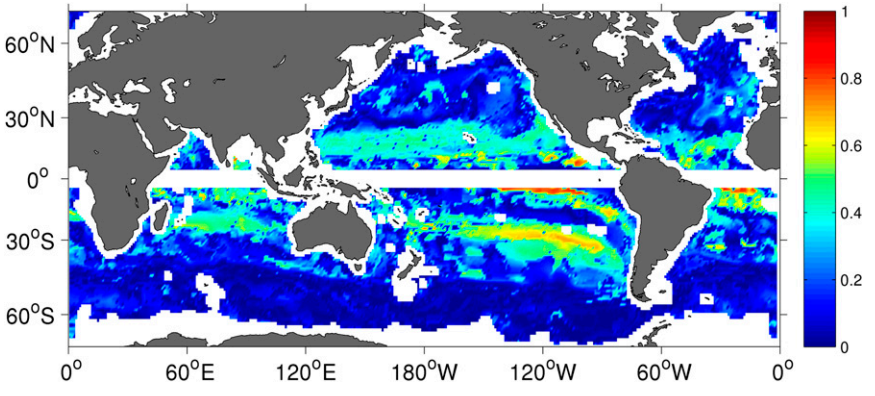

FIG. 14. As in Fig. 13, but for the second baroclinic mode.

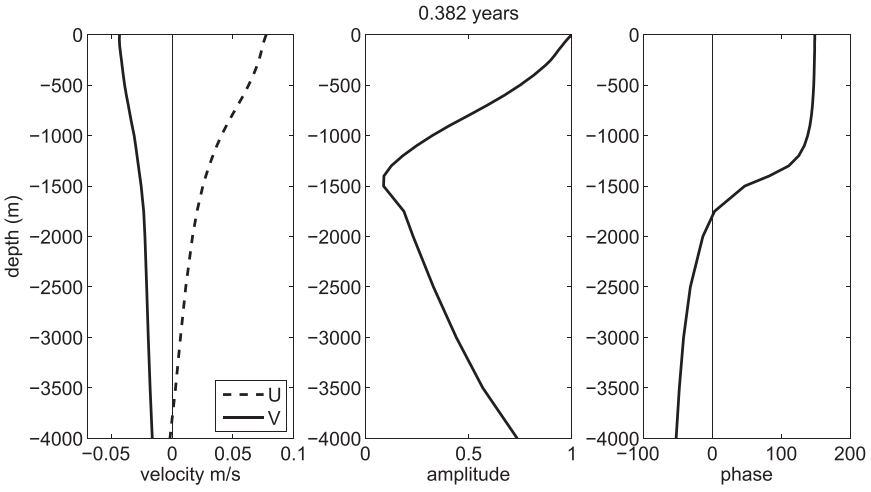

FIG. 15. Vertical structure of the most unstable mode (growth time of 0.382 yr) of the (left) zonal and meridional mean velocities at 51°S and 124°E (ACC) and the (center) amplitude and (right) phase.

unstable region of Fig. 11. The zonal velocity is still eastward at the surface but turns westward at 100-m depth and then eastward again around 2000 m; its projection on the second baroclinic mode is now positive. The most unstable mode has a vertical structure that looks like a second baroclinic mode (it has two zeros on the vertical) and a growth time much longer than before: 3.6 yr. This site where the instability is weak is typical of the midlatitude regions (mainly the central parts of the subtropical gyres) where the zonal mean flow projects negatively on the second baroclinic mode.

f. South Pacific, low-latitude region

The third site is typical of a large part of the unstable region of Fig. 11: low latitudes with westward mean surface current. Figure 17 shows that the mean zonal velocity is westward for all depth with a maximum around 100 m. The meridional mean current is northward with an amplitude smaller than that of the zonal one. The corresponding most unstable mode has a first baroclinic vertical structure, with one zero around 1500 m. The growth time is around 0.3 yr.

These three examples confirm that the largest growth rates are found in mean flows with a negative projection on the second baroclinic mode.

5. Conclusions

We have investigated here large-scale baroclinic instabilities as a potential source of Rossby waves and

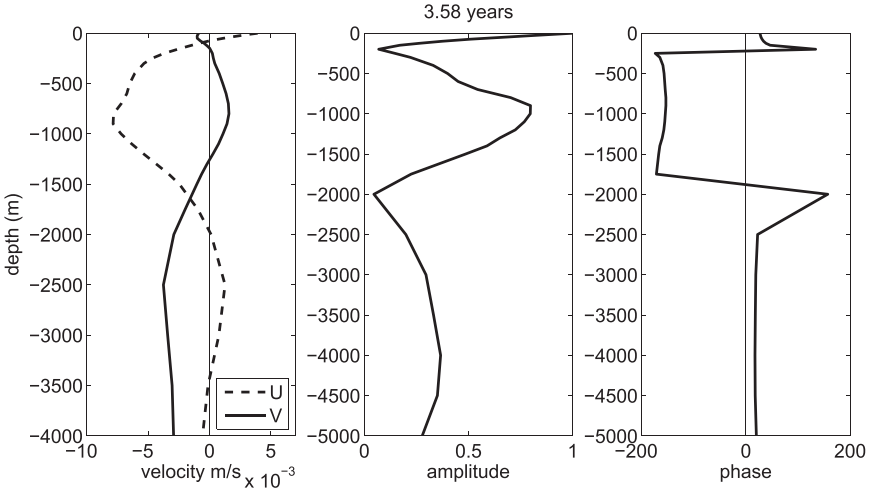

FIG. 16. As in Fig. 15, but for 47°S and 124°E (ACC). Growth time is 3.58 yr.

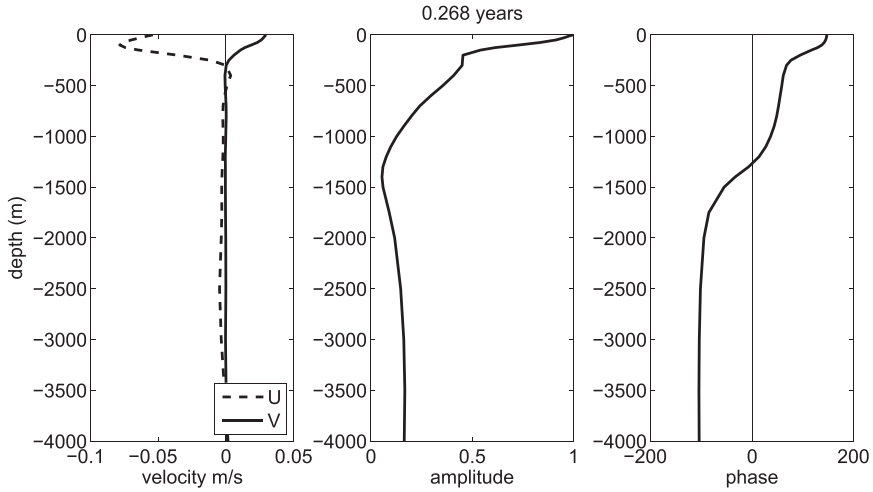

FIG. 17. As in Fig. 15, but for 10.5°S and 120°W (South Pacific, low latitude). Growth time is 0.268 yr.

large-scale ocean variability. We first showed that in a 2.5-layer quasigeostrophic model, the large-scale instability occurs when the projections of the zonal mean flow on the first and second baroclinic modes are both negative (by convention, the vertical modes are positive at the surface). The instability can either occur when the mean flow decelerates the first baroclinic mode toward the second or when the second is accelerated toward the first, a case that has not been described by Liu (1999). Unlike the instability active at mesoscales (Smith 2007), this large-scale instability is stronger at low latitudes. We showed that in the 2.5-layer model the curves of constant phase speed for stable modes, in the (U_1, U_2) plane, are tangent lines to the parabola of neutral stability. The slope of these curves can be linked to the vertical structure of the corresponding modes. The 2.5-layer model is singular; there is no instability along the vertical modes' directions since the non-Doppler shift imposes that one of the phase velocity is real. We thus examined the effect of a larger number of vertical modes using the continuous equations. The calculation reveals that the instabilities are much stronger when the projection on the second baroclinic mode is negative, whereas the projection on the first mode can either be positive or negative. Further investigation shows that the unstable shear modes have a first or second stratification baroclinic mode vertical structure.

The local stability analysis has then been performed on the observed mean flows (U and V), obtained from a reconstruction of the circulation using Argo float displacement at 1000 db and thermal wind, with the quasigeostrophic equation under the long-wave approximation. The results reveal that the most unstable regions are situated at low latitudes, in western boundary currents (particularly in the Gulf Stream), and also at high latitudes in the Antarctic Circumpolar Current. The regions of negative projection of the mean flow on the second baroclinic mode are also situated at low latitudes in every oceanic basin and in the Antarctic Circumpolar Current and correlate well with the regions of largest growth. The growth time scales at low latitudes are generally shorter than a year for length scales of a thousand kilometers and are thus likely to contribute to the generation of the Rossby waves that can be observed in these regions. Our results significantly differ from the Charney-type baroclinic instability growth rate close to or below the internal Rossby radius scale (Smith 2007). Two types of regions show relatively large growth rates at both wavelengths, the western boundary current regions (Gulf Stream and Kuroshio) and the ACC. Otherwise, the latitude dependence of the growth rate at mesoscale and large-scale appears clearly different: low latitudes show the smaller growth at the mesoscale, but larger growth at the large scale. The next section discusses these results and suggests several improvements of this work.

6. Discussion

This article examines the potential generation of large-scale variability by baroclinic instability. Since the zonal phase speed of the unstable modes is comparable to that of the observed phase speed at low latitudes, the observed signal in this region could be the result of unstable Rossby waves. Further investigations are needed to answer this question. The time scales under consideration here are thus around a year. Since the employed methodology—the linear stability analysis—has a lot in

common with the one used to calculate the basin modes, it is worth comparing the location of the unstable region found here with the location of the largest amplitude of the basin modes. We recall that the oceanic basin modes, thanks to their multidecadal time scales, are one of the proposed explanations for interdecadal climate variability.

In Sévellec and Fedorov (2013), the basin modes are calculated using a realistic simulation of the North Atlantic and a tangent linear model. The authors showed that the least damped mode of their model has a maximum amplitude north of Newfoundland and south of Greenland. This result is in reasonable agreement with the location of the low frequency found in the idealized studies of Colin de Verdière and Huck (1999) and Huck et al. (2001). Since our local calculation shows that the unstable regions are situated mainly at low latitudes and certainly not north of Newfoundland, we therefore ask the following question: what is the link between the basin modes and the local unstable modes? The answer to this question will be of great interest since the dynamics of the local mode is relatively simple to understand (as shown in this article), whereas the detailed dynamics of the basin modes is quite opaque.

To progress in this direction, one needs to identify in the equations of motion the terms that need to be added to continuously transform the local modes into the basin modes. The following terms are likely to play a role and need to be studied: realistic boundary conditions, horizontally variable mean flow, varying Coriolis parameter, dissipation and diffusion, and spherical coordinates.

Acknowledgments. We thank the two anonymous reviewers for improving the original version of this manuscript.

REFERENCES

Antonov, J. I., and Coauthors, 2010: *Salinity*. Vol. 2, *World Ocean Atlas 2009*, NOAA Atlas NESDIS 69, 184 pp.

Aoki, K., A. Kubokawa, H. Sasaki, and Y. Sasai, 2009: Mid-latitude baroclinic Rossby waves in a high-resolution OGCM simulation. *J. Phys. Oceanogr.*, **39**, 2264–2279, doi:10.1175/2009JPO4137.1.

Bobrovich, A., and G. Reznik, 1999: Planetary waves in a stratified ocean of variable depth. Part 2. Continuously stratified ocean. *J. Fluid Mech.*, **388**, 147–169, doi:10.1017/S0022112099004863.

Cabanes, C., T. Huck, and A. Colin de Verdière, 2006: Contributions of wind forcing and surface heating to interannual sea level variations in the Atlantic Ocean. *J. Phys. Oceanogr.*, **36**, 1739–1750, doi:10.1175/JPO2935.1.

Charney, J. G., 1947: The dynamics of long waves in a baroclinic westerly current. *J. Meteor.*, **4**, 136–162, doi:10.1175/1520-0469(1947)004<0136:TDOLWI>2.0.CO;2.

Chelton, D. B., and M. G. Schlax, 1996: Global observations of oceanic Rossby waves. *Science*, **272**, 234–238, doi:10.1126/science.272.5259.234.

Colin de Verdière, A., 1986: On mean flow instabilities within the planetary geostrophic equations. *J. Phys. Oceanogr.*, **16**, 1981–1984, doi:10.1175/1520-0485(1986)016<1981:OMFIWT>2.0.CO;2.

——, and T. Huck, 1999: Baroclinic instability: An oceanic wavemaker for interdecadal variability. *J. Phys. Oceanogr.*, **29**, 893–910, doi:10.1175/1520-0485(1999)029<0893:BIAOWF>2.0.CO;2.

——, and R. Tailleux, 2005: The interaction of a baroclinic mean flow with long Rossby waves. *J. Phys. Oceanogr.*, **35**, 865–879, doi:10.1175/JPO2712.1.

de Szoeke, R. A., 1999: An improved bound for the complex phase speed of baroclinic instability. *J. Phys. Oceanogr.*, **29**, 83–91, doi:10.1175/1520-0485(1999)029<0083:AIBFTC>2.0.CO;2.

Dewar, W., 1998: On ''too fast'' baroclinic planetary waves in the general circulation. *J. Phys. Oceanogr.*, **28**, 1739–1758, doi:10.1175/1520-0485(1998)028<1739:OTFBPW>2.0.CO;2.

Flierl, G., 1978: Models of vertical structure and the calibration of two-layer models. *Dyn. Atmos. Oceans*, **2**, 341–381, doi:10.1016/0377-0265(78)90002-7.

Fu, L.-L., 2004: Latitudinal and frequency characteristics of the westward propagation of large-scale oceanic variability. *J. Phys. Oceanogr.*, **34**, 1907–1921, doi:10.1175/1520-0485(2004)034<1907:LAFCOT>2.0.CO;2.

——, and A. Cazenave, 2000: *Satellite Altimetry and Earth Sciences: A Handbook of Techniques and Applications.* International Geophysics Series, Vol. 69, Academic Press, 463 pp.

——, and B. Qiu, 2002: Low-frequency variability of the North Pacific Ocean: The roles of boundary- and wind-driven baroclinic Rossby waves. *J. Geophys. Res.*, **107**, 3220, doi:10.1029/2001JC001131.

Gill, A., J. Green, and A. Simmons, 1974: Energy partition in the large-scale ocean circulation and the production of mid-ocean eddies. *Deep-Sea Res. Oceanogr. Abstr.*, **21**, 499–528, doi:10.1016/0011-7471(74)90010-2.

Green, J., 1960: A problem in baroclinic stability. *Quart. J. Roy. Meteor. Soc.*, **86**, 237–251, doi:10.1002/qj.49708636813.

Huck, T., G. K. Vallis, and A. Colin de Verdière, 2001: On the robustness of the interdecadal modes of the thermohaline circulation. *J. Climate*, **14**, 940–963, doi:10.1175/1520-0442(2001)014<0940:OTROTI>2.0.CO;2.

Hunt, F., R. Tailleux, and J.-M. Hirschi, 2012: The vertical structure of oceanic Rossby waves: A comparison of high-resolution model data to theoretical vertical structures. *Ocean Sci.*, **8**, 19–35, doi:10.5194/os-8-19-2012.

Killworth, P. D., and J. R. Blundell, 2005: The dispersion relation for planetary waves in the presence of mean flow and topography. Part II: Two-dimensional examples and global results. *J. Phys. Oceanogr.*, **35**, 2110–2133, doi:10.1175/JPO2817.1.

——, and ——, 2007: Planetary wave response to surface forcing and instability in the presence of mean flow and topography. *J. Phys. Oceanogr.*, **37**, 1297–1320, doi:10.1175/JPO3055.1.

——, D. B. Chelton, and R. A. de Szoeke, 1997: The speed of observed and theoretical long extratropical planetary waves. *J. Phys. Oceanogr.*, **27**, 1946–1966, doi:10.1175/1520-0485(1997)027<1946:TSOOAT>2.0.CO;2.

Liu, Z., 1999: Planetary wave modes in the thermocline: Non-Doppler-shift mode, advective mode and green mode. *Quart. J. Roy. Meteor. Soc.*, **125**, 1315–1339, doi:10.1002/qj.1999.49712555611.

Locarnini, R. A., A. V. Mishonov, J. I. Antonov, T. P. Boyer, H. E. Garcia, O. K. Baranova, M. M. Zweng, and D. R. Johnson, 2010: *Temperature*. Vol. 1, *World Ocean Atlas 2009*, NOAA Atlas NESDIS 68, 184 pp.

Ollitrault, M., and A. Colin de Verdière, 2014: The ocean general circulation near 1000-m depth. *J. Phys. Oceanogr.*, **44**, 384–409, doi:10.1175/JPO-D-13-030.1.

Osychny, V., and P. Cornillon, 2004: Properties of Rossby waves in the North Atlantic estimated from satellite data. *J. Phys. Oceanogr.*, **34**, 61–76, doi:10.1175/1520-0485(2004)034<0061:PORWIT>2.0.CO;2.

Polito, P. S., and W. T. Liu, 2003: Global characterization of Rossby waves at several spectral bands. *J. Geophys. Res.*, **108**, 3018, doi:10.1029/2000JC000607.

Sévellec, F., and A. V. Fedorov, 2013: The leading, interdecadal eigenmode of the Atlantic meridional overturning circulation in a realistic ocean model. *J. Climate*, **26**, 2160–2183, doi:10.1175/JCLI-D-11-00023.1.

——, and T. Huck, 2015: Theoretical investigation of the Atlantic multidecadal oscillation. *J. Phys. Oceanogr.*, **45**, 2189–2208, doi:10.1175/JPO-D-14-0094.1.

Smith, K. S., 2007: The geography of linear baroclinic instability in Earth's oceans. *J. Mar. Res.*, **65**, 655–683, doi:10.1357/002224007783649484.

Spall, M. A., 2000: Generation of strong mesoscale eddies by weak ocean gyres. *J. Mar. Res.*, **58**, 97–116, doi:10.1357/002224000321511214.

Tailleux, R., and J. C. McWilliams, 2001: The effect of bottom pressure decoupling on the speed of extratropical, baroclinic Rossby waves. *J. Phys. Oceanogr.*, **31**, 1461–1476, doi:10.1175/1520-0485(2001)031<1461:TEOBPD>2.0.CO;2.

White, W. B., and J. Saur, 1983: Sources of interannual baroclinic waves in the eastern subtropical North Pacific. *J. Phys. Oceanogr.*, **13**, 531–544, doi:10.1175/1520-0485(1983)013<0531:SOIBWI>2.0.CO;2.

Zang, X., and C. Wunsch, 2001: Spectral description of low-frequency oceanic variability. *J. Phys. Oceanogr.*, **31**, 3073–3095, doi:10.1175/1520-0485(2001)031<3073:SDOLFO>2.0.CO;2.